Applied Physics A (2018) 124:215
https://doi.org/10.1007/s00339-018-1657-7

**Applied Physics A**
**Materials Science & Processing**

# Photoluminescence and cathodoluminescence of Mn doped zinc silicate nanophosphors for green and yellow field emissions displays

**K. Omri[1] · A. Alyamani[2] · L. El Mir[1,3]**

Received: 20 December 2017 / Accepted: 5 February 2018 / Published online: 7 February 2018


**Abstract**
$Mn^{2+}$-doped $Zn_2SiO_4$ ($ZSM^{2+}$) was synthesized by a facile sol–gel technique. The obtained samples were characterized by X-ray diffraction (XRD), Raman spectroscopy, photoluminescence (PL) and cathodoluminescence (CL) techniques. Under UV excitation, spectra showed that the α-$ZSM^{2+}$ phosphor exhibited a strong green emission around 525 nm and reached the highest luminescence intensity with the Mn doping concentration of 5 at.%. However, for the β-$ZSM^{2+}$ phase, an interesting yellow emission band centered at ~ 575 nm of $Mn^{2+}$ at the $Zn^{2+}$ tetrahedral sites was observed. In addition, an unusual red shift with increasing $Mn^{2+}$ content was also found and attributed to an exchange interaction between $Mn^{2+}$. Both PL and CL spectra exhibit an intense green and yellow emission centered at ~ 525 and ~ 573 nm, respectively, due to the $^4T_1$ ($^4G$)-$^6A_1$ ($^6S$) transition of $Mn^{2+}$. Furthermore, these results indicated that the $Mn^{2+}$-doped zinc silicate phosphors may have potential applications in green and yellow emissions displays like field emission displays (FEDs).

## 1 Introduction

In the development of field emission display (FED) phosphors, new constraints compared with conventional cathode ray tube (CRT) phosphors should be overcome [1]. Thus, many researches have tried to reduce the surface resistance of phosphor by coating some conducting materials [2–4]. The characteristics of phosphor are important to maximize the luminous efficiency of displays [2]. That is, the visible light generated must be ejected from the phosphor material with a minimum loss. Such extraction efficiency of the light is strongly affected by the characteristics of phosphor. The particle size and the shape of phosphor directly affect the properties such as surface uniformity, and microstructure [3]. These properties determine the characteristics of the pathway for the generated light when it going out of the phosphor [4].

To get high-quality yellow emission, manganese (Mn) is considered as one of the most conventional phosphor activators due to its bright yellow emission at ~ 575 nm originating from the 3d transition which is dependent on symmetric sites [5]. The chemical similarity between $Zn^{2+}$ and $Mn^{2+}$ facilitates the incorporation of the dopant ion; a lot of studies have been done on $ZSM^{2+}$ phosphor. Since a significant part of the $Mn^{2+}$ ions resides near the surface of the phosphor, the incorporated concentration of $Mn^{2+}$ is consistently lower than the intended dopant concentration [6]. It is wellknown that several phosphors such as $NaLaMgWO_6:Dy^{3+}$ and $Sr_8CaBi(PO_4)_7:Eu^{2+}$ have been investigated as the commercial yellow-emitting phosphors [7, 8]. Unfortunately, these kinds of phosphors suffer from some drawbacks such as poor stability and special reaction environment.

Currently, the phosphor materials, which exhibit a common structure of phosphor, have attracted great interest in various optoelectronic applications because of their excellent luminescence properties and their availability in nature [7–9]. In particular, Mn-doped zinc silicate ($ZSM^{2+}$) materials containing peculiar optical characters are regarded as promising candidates for luminescent materials [10–12]. El Mir et al. [13], studied the structural and photoluminescence properties of α- and β-$ZSM^{2+}$ material and confirmed that

✉ K. Omri
omrikarim16@yahoo.fr

[1] Laboratoire de Physique des Matériaux et des Nanomatériaux Appliquée à l'Environnement, Faculté des Sciences de Gabès, Cité Erriadh Manara Zrig, 6072 Gabès, Tunisia

[2] National Nanotechnology Research Centre, KACST, Riyadh, Saudi Arabia

[3] Department of Physics, College of Sciences, Al Imam Mohammad Ibn Saud Islamic University (IMSIU), Riyadh 11623, Saudi Arabia

α- and β-$ZSM^{2+}$ show luminescence depending on their crystal structure.

Mai et al. [14], studied the optical properties of $ZSM^{2+}$ material and confirmed that the photoluminescence indicates $Mn^{2+}$-related emission at an average wavelength of 579 and 528 nm. Mbule et al. [15] have reported the factors influencing luminescent properties of Mn doped zinc silicate phosphors prepared by sol–gel and combustion methods. They have studied the fast and slow decay components that are due to the pair or cluster formation and isolated ions at higher doping concentration, respectively [14, 16]. Being based on analysis of the luminescence spectrum, it has been shown that emission band assigned to the $^4T_1(^4G) \rightarrow {}^6A_1(^6S)$ electronic transition of $Mn^{2+}$ was observed with maximum intensity at ~ 573 nm for combustion samples and ~ 532 nm for sol–gel samples [16] .

The dependence of PL and CL of $ZSM^{2+}$ nanophosphors on the particle size is not satisfactorily understood to date. In our previous study on the preparation of $SZM^{2+}$ nanophosphors by sol–gel method [17], we introduced a solution technique which made it possible to successfully obtain homogene particles with a dense structure. The nanophosphors were characterized by various techniques. In the present work, to understand the origin of the luminescence and the small shift generally observed, additional characterizations have been considered, including Roman and cathodoluminescence (CL).

## 2 Experimental procedure

### 2.1 Preparation of ZSMn nanophosphors

The α- and β-$ZSMn^{2+}$ nanophosphors were prepared by a sol–gel process under supercritical conditions of ethyl alcohol (EtOH) based on K. Omri et al. protocol [17].

### 2.2 Characterization

The crystalline phases of our samples were identified by X-ray diffraction (XRD) using a Bruker D5005 powder X-ray diffractometer with a CoKα source ($\lambda = 1.78901$ Å). Crystallite size ($G$, in Å) were estimated from the Scherrer's equation (Eq. 1) [18]:

$$G = \frac{0.9\lambda}{B\cos\theta_B}, \quad (1)$$

where $\lambda$ is the X-ray wavelength (1.78901 Å), $\theta_B$ is the maximum of the Bragg diffraction peak (in radians) and B is the line-width at half maximum. Transmission electron microscopy (TEM, JEM-200CX) was used to study the morphology and particle size of the phosphor powders. Raman scattering spectra were collected on a Laser Confocal Microscopy Raman Spectrometer (Lab RAM HR Evolution) with a He–Cd laser (wavelength of 532 nm) for the excitation. For PL measurements, the 450-W Xenon lamp was used as an excitation source. CL study was investigated using a Gatan MonoCL4 operated at 10 kV. The magnetic properties of the nanophosphor samples were characterized by a commercial Quantum Design SQUID-VSM magnetometer.

## 3 Results and discussion

### 3.1 Raman spectral analysis

Figure 1 shows the Raman spectra of the samples α-$ZSMn^{2+}$ and β-$ZSMn^{2+}$ nanophosphors at room temperature. All of Raman spectra exhibited strong characteristic modes of vibration; three intense modes of vibration at 852, 902 and 946 $cm^{-1}$ for α-$ZSMn^{2+}$ nanophosphors and also three intense modes of vibration at 867, 929 and 964 $cm^{-1}$ for

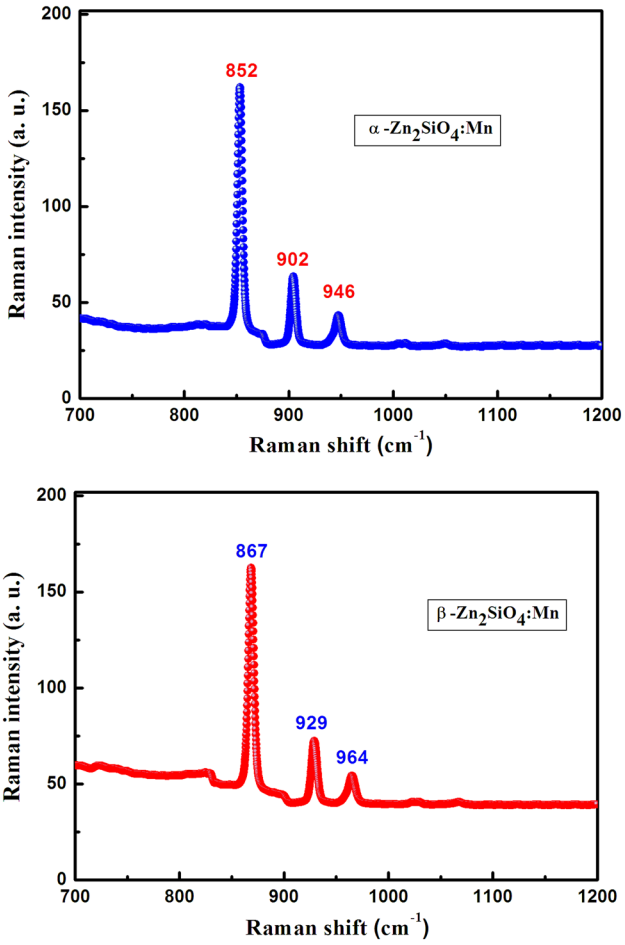


**Fig. 1** Raman spectra of the α-$ZSMn^{2+}$ and β-$ZSMn^{2+}$ nanophosphors

β-ZSMn$^{2+}$ [19]. Raman bands between 800 and 1100 cm$^{-1}$ were assigned to stretching and flexing bands of $SiO_4$ groups, respectively [19]. In our case, of heavy doping with $Mn^{2+}$ ions, the additional Raman peak positions coincide exactly with those of ZSMn$^{2+}$, which is not detectable in Raman due to small limitation of the measurement. These results further proved the formation of the ZSMn$^{2+}$ phase, which were well consistent with the XRD results.

### 3.2 Structural studies

Figure 2 shows the TEM images and XRD spectra of α-ZSMn$^{2+}$ and β-ZSMn$^{2+}$ nanophosphors. TEM images show well-structured zinc silicate (ZS) particles of small and round grains with an average diameter of about 80 nm. The images depict the irregular distribution of the size but in all cases they are in the nanometer range. The weak aggregation found between particles is due to the calcinations at high temperature. The micrographs reveal that, the phosphor show highly agglomerated, porous, irregular size particles. It can be observed that the agglomerated particles have no uniform shape and size. This non uniformity is related to the non-uniform distribution of the heating temperature. This characteristic was also confirmed by the XRD as shown in Fig. 2. In fact; XRD is the finest convenient method for characterizing the crystallinity and phase purity of the samples. The powder X-ray diffraction patterns of α-ZSMn$^{2+}$ and β-ZSMn$^{2+}$ nanophosphors have been presented. Some of diffraction peaks become narrower and sharper than that of original ones, reflection peaks could be identified clearly due to the growth of α-ZSM and β-ZSM particles, which matches well to that JCPDS No. 37-1485 and JCPDS no. 19-1479 Cards, respectively [20]. According to our earlier reports [13, 17], the optimum temperature was found at 1200 °C for α-ZSMn$^{2+}$ and the reduction of doping concentrations show a considerable effect on the size and phase of crystallites purity [16]. The XRD pattern was in good agreement with the data of Marit Maiet et al. [14] who confirmed that the diffraction peaks correspond to typical rhombohedral ZS phase with the $R\bar{3}$ space group and cell parameters of *a*

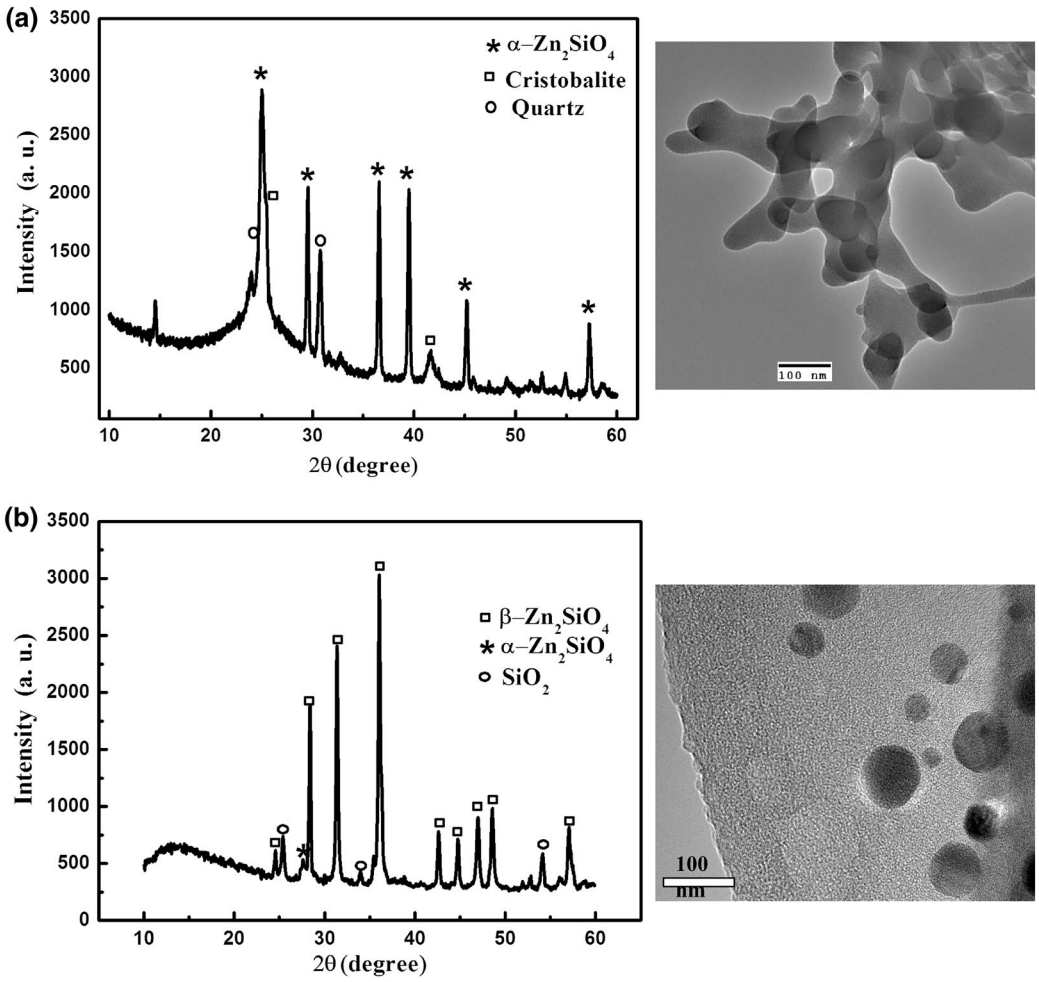


**Fig. 2** X-ray diffraction pattern and TEM photograph showing the general morphology of the **a** α-ZSMn$^{2+}$ and **b** β-ZSMn$^{2+}$ nanophosphors

= 13.944 and $c = 9.315$ Å. With the introduction of dopants ($Mn^{2+}$), as shown in Fig. 2, the XRD patterns were almost similar, indicating the high single crystallinity without significant change of host structures by dopants. This result indicates that α-ZS has a rhombohedral structure [13]. These nanophosphors β-ZS$Mn^{2+}$ crystallize in triclinic structure [15]. The size of the particles from samples, calculated from the Scherrer's formula (Eq. 1) is typically 85 nm [19]. The range of crystallite size obtained from XRD nearly agrees with the particle size obtained from the TEM studies.

## 3.3 Optical properties

### 3.3.1 Fourier transform infrared spectroscopy (FTIR)

The formation and purity of the α-ZS$Mn^{2+}$ and β-ZS$Mn^{2+}$ nanophosphors synthesized by sol–gel method were further confirmed by FTIR studies and results were depicted in Fig. 3. The FTIR spectra of α-ZS$Mn^{2+}$ sample are shown in Fig. 3 where the totally symmetric stretching bands at 576 $cm^{-1}$ ($\upsilon_1$ $ZnO_4$; symmetric stretching), 461 $cm^{-1}$ ($\upsilon_4$ $SiO_4$; asymmetric deformation), 901, 941 and 974 $cm^{-1}$ ($\upsilon_3$ $SiO_4$; asymmetric stretching), 863 $cm^{-1}$ ($\upsilon_1$ $SiO_4$; symmetric stretching) [21] confirming the formation of the SZ phase. In the case of β-ZS$Mn^{2+}$ nanophosphors, the bands were observed at 578 $cm^{-1}$ ($\upsilon_1$ $ZnO_4$; symmetric stretching), 463 $cm^{-1}$ ($\upsilon_4$ $SiO_4$; asymmetric deformation), 913, 963 and 984 $cm^{-1}$ ($\upsilon_3$ $SiO_4$; asymmetric stretching), 868 $cm^{-1}$ ($\upsilon_1$ $SiO_4$; symmetric stretching). The intensity of the band due to symmetric stretching ($\upsilon_3$ $SiO_4$) and asymmetric deformation ($\upsilon_4$ $SiO_4$) reduced appreciably. Additionally, the symmetric stretching ($\upsilon_1$ $ZnO_4$) shifted to 578 $cm^{-1}$ [22]. The formation of both Zn and Si vacancies at high temperature is the driving force for the rapid formation SZ and the silicate phases. However it will be necessary to follow the formation of the different phases observed, as the temperature is raised, to obtain a better understanding of the changes that occur.

### 3.3.2 Photoluminescence properties

Figure 4 shows the room-temperature photoluminescence spectra of α-ZS$Mn^{2+}$ and β-ZS$Mn^{2+}$ nanophosphors synthesized by sol–gel method. The emission spectra of our nanophosphors under 255 nm excitation consist of a wide green band with a peak at about 525 nm for α-ZS$Mn^{2+}$ sample and yellow emission at 575 nm for β-ZS$Mn^{2+}$ phase, which are due to a $3d^5$ ($^4T_{1g}$)–$3d^5$ ($^6A_{1g}$) transition corresponds of $Mn^{2+}$ ions in different phases [23]. As shown in Fig. 5, α-ZS$Mn^{2+}$ sample have broad photoluminescence band with intensity depends on measurement temperature. The green luminescence of α-phase with the maximum PL wavelength at 525 nm could be found. The $Mn^{2+}$ ion substitutes for $Zn^{2+}$ in the ZS lattice due to similar ionicity. Annealing at high temperature is an effective way to improve the emission intensities of the phosphor because it reduces the surface

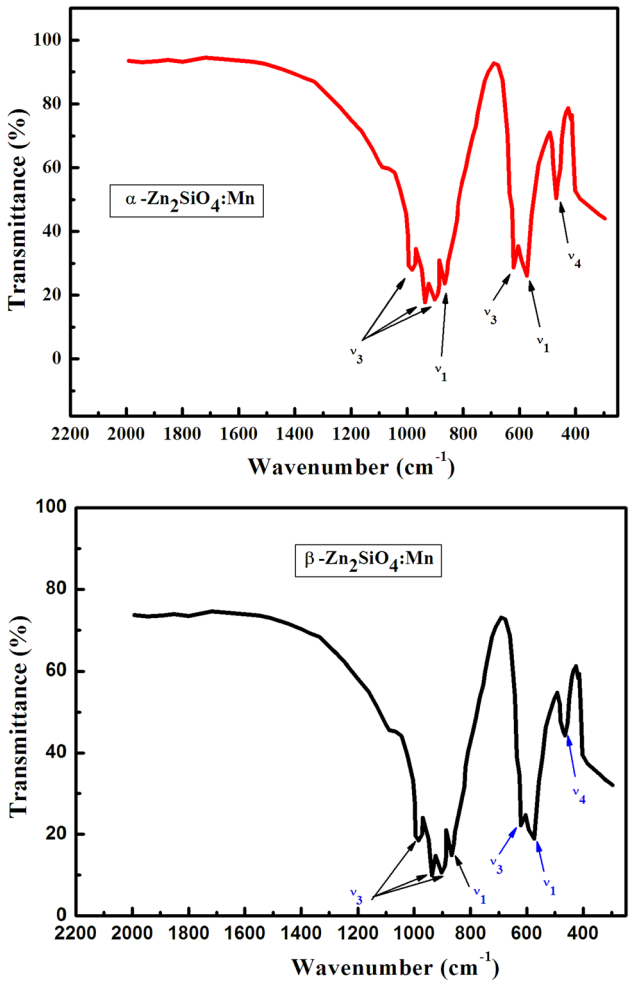


**Fig. 3** FTIR spectra of α-ZS$Mn^{2+}$ and β-ZS$Mn^{2+}$ nanophosphors

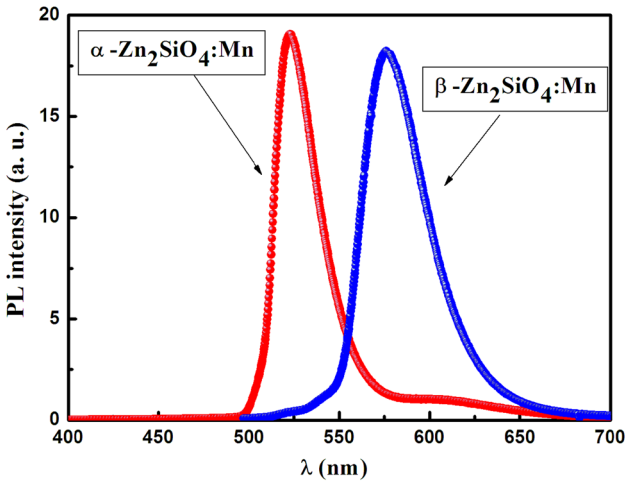


**Fig. 4** PL spectra of α-ZS$Mn^{2+}$ and β-ZS$Mn^{2+}$ nanophosphors

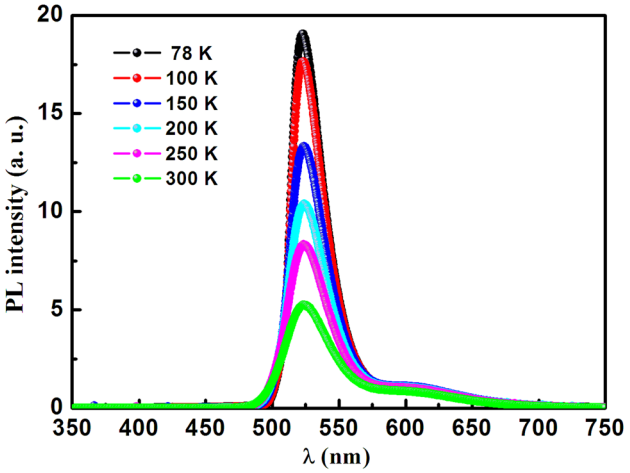


**Fig. 5** PL spectra of the α-$ZSMn^{2+}$ nanophosphors at different temperatures

defects and improves crystallinity. But with the d electrons within the 3d sublayer, $Mn^{2+}$ emission can be affected by the crystal field, which results in the emission changing from green to red.

Figure 6 shows the PL emission spectra of β-$ZSMn^{2+}$ nanophosphors at different temperatures, measured at an excitation wavelength of 255 nm. The result indicates that the yellow emissions come from the same source, namely, the transition from $^4T_1$ ($^4G$) → $^6A_1$ ($^6S$) of the doping $Mn^{2+}$ ions substituted in $Zn^{2+}$ sites of the ZS lattice [15, 17]. Additionally, when $Mn^{2+}$ is located in the tetrahedral crystal field, it can emit green light. In other words, through changing the crystal field conditions, the spin forbidden d–d in $Mn^{2+}$ transition ($^4T_1 - {}^6A_1$) can emit green light [13].

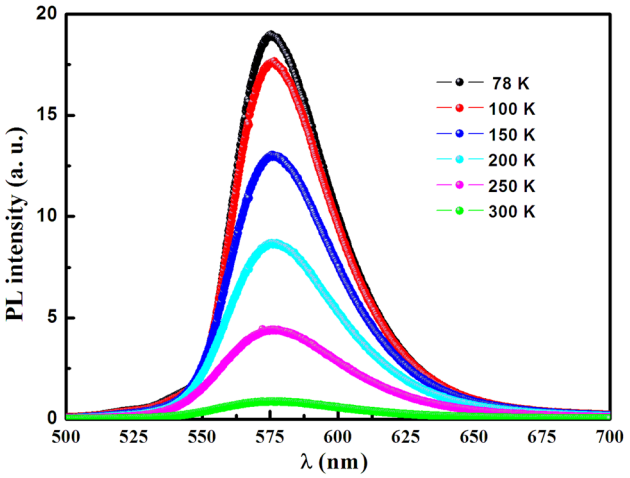


**Fig. 6** PL spectra of the β-$ZSMn^{2+}$ nanophosphors at different temperatures

### 3.3.3 CL properties of $ZSM^{2+}$

The spectra are similar to that of PL. As a typical sample, the CL spectra of α-$ZSMn^{2+}$ and β-$ZSMn^{2+}$ nanophosphors are shown in Fig. 7. Under (10 kV and 70 mA) excitation, the emission spectrum consists of a dominant band at 526 nm (α-$ZSMn^{2+}$) and 574 nm (β-$ZSMn^{2+}$), due to the $^4T_1$ ($^4G$) → $^6A_1$ ($^6S$) transition of $Mn^{2+}$ [24]. For α-$ZSMn^{2+}$ sample, its FWHM is ~ 80 nm. The measured CL spectrum exhibited high similarity with the PL spectra in Fig. 5. Compared with this spectrum, it is obvious that CL emission is wider and exhibits a small blue shift. However, in the case of β-$ZSMn^{2+}$ nanophosphors, the surface of the phosphor did not fully react with the Zn ions, probably because of the high temperature of the Zn ions. Although the CL behaviors of Mn doped $ZSMn^{2+}$ phosphors are not fully understood at present, the precise control of Zn ions into the phosphor surface depending on its sintering conditions will be helpful in terms of increasing CL [25].

## 3.4 Magnetic properties

$ZSMn^{2+}$ samples have promising applications in bioimaging and drug delivery [55]. The magnetic properties of the samples are investigated by VSM. The Magnetic moment versus magnetic field (M−H) curve of $ZSMn^{2+}$ nanophosphors has been studied at 300 and 5 K by SQUID and the result is presented in Fig. 8. At 300 K, the curves show that there is a ferromagnetic component superimposed on strong diamagnetic backgrounds (Fig. 8a). In addition, at 5 K the magnetization curves show that our nanophosphors have both paramagnetic behaviors. The values of the saturation magnetization ($M_s$) of α-$ZSMn^{2+}$ and β-$ZSMn^{2+}$ nanophosphors are 0.0021 and 0.0019 emu/g, respectively. The values of the coercive field ($H_c$) deduced from the measurements

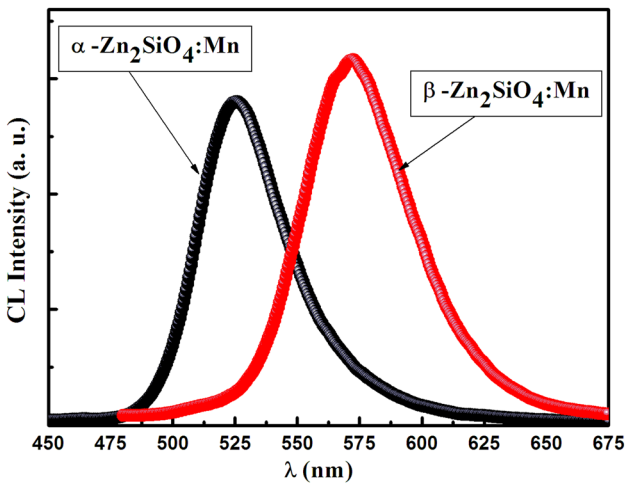


**Fig. 7** CL spectra of α-$ZSMn^{2+}$ and β-$ZSMn^{2+}$ nanophosphors

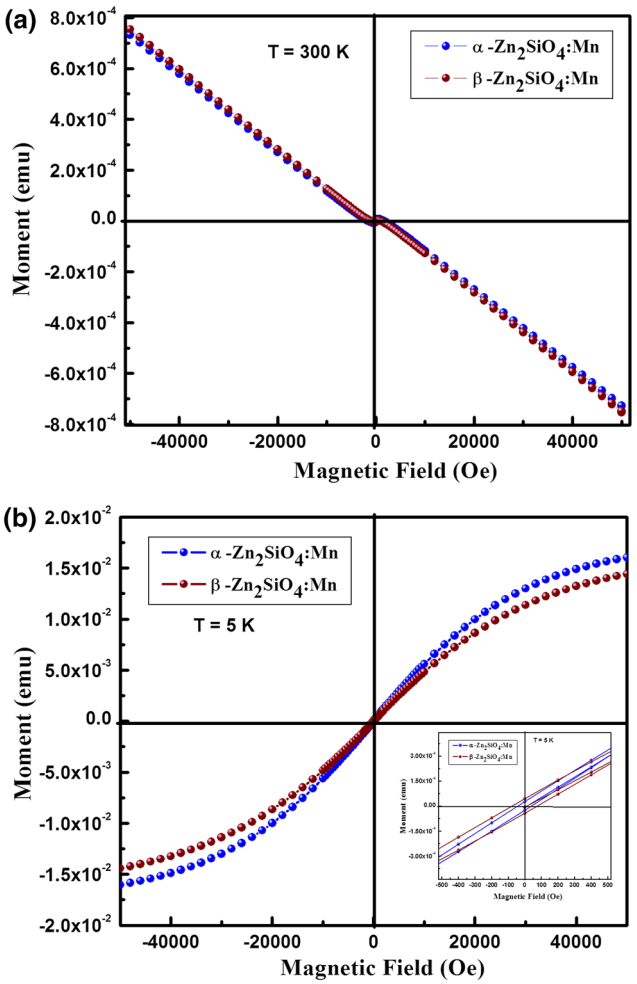


**Fig. 8** M-H curves of ZSMn nanophosphors at 5 and 300 K

are 92.7 and 91.8 Oe, respectively. It can be seen that the saturation magnetization value at room temperature is lower than the value obtained at 5 K [26].

## 4 Conclusion

The $ZSMn^{2+}$ samples nanophosphors were synthesized by sol–gel method. The PL exhibited green and yellow emissions of $Mn^{2+}$ ion attributed due to the $^4T_1$ ($^4G$) – $^6A_1$ ($^6S$) transitions under 255 nm wavelength excitation. Furthermore, the $ZSMn^{2+}$ nanophosphors possessed excellent CL emission intensity that could be significantly enhanced with elevating the accelerating voltage and filament current. Nevertheless, the magnetic properties of our samples show that there is a ferromagnetic component superimposed on strong diamagnetic and paramagnetic depend with temperature. These characteristics make the α-$ZSMn^{2+}$ and β-$ZSMn^{2+}$ nanophosphors promising candidates for white LEDs and FEDs as green and yellow emitting phosphors.

## References


1. Y. Zhou, J. Lin, S. Wang, Energy transfer and upconversion luminescence properties of $Y_2O_3$:Sm and $Gd_2O_3$:Sm phosphors. J. Solid State Chem. **171**, 391–395 (2003)
2. K. Youl Jung, K. Hyun Han, Y. Soo, Ko, Cathodoluminescence characteristics of particles and film of $(Y, nZn)_2O_3$:Eu phosphor prepared by spray pyrolysis. J. Luminescence. **127**, 391–396 (2007)
3. R. Mlcak, A.H. Kitai, Cathodoluminescence of $Mn^{2+}$ centers in $MgAl_2O_4$ spinels. J. Luminescence. **46**, 391–396 (1990)
4. G.Q. Xu, H.T. Xu, Z.X. Zheng, Y.C. Wu, Preparation and characterization of $Zn_2SiO_4$:Mn phosphors with hydrothermal methods. J. Luminescence. **130**, 1717–1720 (2010)
5. J. El Ghoul, I. Ghiloufi, L. El, Mir, Effect of annealing temperature on the luminescence properties of $Zn_2SiO_4$:V nanocomposite. J. Luminescence. **170**, 288–292 (2016)
6. K.W. Park, H.S. Lim, S.W. Park, G. Deressa, J.S. Kim, Strong blue absorption of green $Zn_2SiO_4$:$Mn^{2+}$ phosphor by doping heavy $Mn^{2+}$ concentrations. Chem. Phys. Lett. **636**, 141–145 (2015)
7. B. Han, Y. Dai, J. Zhang, H. Shi, Luminescence properties of a novel yellow-emitting phosphor $NaLaMgWO_6$:$Dy^{3+}$. Mater. Lett. **204**, 145–148 (2017)
8. Q. Zhang, X. Wang, X. Ding, Y. Wang, A broad band yellow-emitting $Sr_8CaBi(PO_4)_7$:$Eu^{2+}$ phosphor for n-UV pumped white light emitting devices. Dyes Pigm. **149**, 268–275 (2018)
9. C. Chen Diao, C. Yang, R. Wang, J. Lin, M. Fu, Prepare high efficiency $Mn^{2+}$-doped $Zn_2SiO_4$ green phosphors in air using nanoparticles. J. Lumin. **131**, 915–920 (2011)
10. S. Imashuku, K. Ono, R. Shishido, S. Suzuki, K. Wagatsuma, Cathodoluminescence analysis for rapid identification of alumina and $MgAl_2O_4$ spinel inclusions in steels. Mater. Charact. **131**, 210–216 (2017)
11. M. Masjedi-Arani, M. Salavati-Niasari, A simple sonochemical approach for synthesis and characterization of $Zn_2SiO_4$ nanostructures. Ultrason. Sonochem. **29**, 226–235 (2016)
12. R. Ye, H. Ma, C. Zhang, Y. Gao, Y. Hua, D. Deng, P. Liu, S. Xu, Luminescence properties and energy transfer mechanism of $Ce^{3+}$/$Mn^{2+}$ co-doped transparent glass-ceramics containing β-$Zn_2SiO_4$ nano-crystals for white light emission. J. Alloy. Compd. **566**, 73–77 (2013)
13. L. El Mir, K. Omri, J. El, Ghoul, Effect of crystallographic phase on green and yellow emissions in Mn-doped zinc silicate nanoparticles incorporated in silica host matrix. Superlattices Microstruct. **85**, 180–184 (2015)
14. M. Mai, C. Feldmann, Two-color emission of $Zn_2SiO_4$:Mn from ionic liquid mediated synthesis. Solid State Sci. **11**, 528–532 (2009)
15. P.S. Mbule, O.M. Ntwaeaborwa, B.M. Mothudi, M.S. Dhlamini, Structural and optical characterization of nanoparticulate manganese doped zinc silicate phosphors prepared by sol–gel and combustion methods. J. Luminescence. **179**, 74–82 (2016)
16. V. Sivakumar, A. Lakshmanan, Pyrolysis synthesis of $Zn_2SiO_4$:$Mn^{2+}$ phosphors—effect of fuel, flux and co-dopants. J. Luminescence. **145**, 420–424 (2014)
17. K. Omri, O.M. Lemine, L. El, Mir, Mn doped zinc silicate nanophosphor with bifunctionality of green-yellow emission and magnetic properties. Ceram. Int. **43**, 6585–6591 (2017)
18. B.D. Cullity, *Elements of X-ray Diffractions* (Addison-Wesley, Reading, MA, 1978), p. 102
19. G. Hu, W. Li, G. He, J. Wang, Y. Zhao, Y. Zhang, B. Yao, Molten salt synthesis of $Zn_{1.8}Mn_{0.2}SiO_4$ luminescent materials in NaCl–$ZnCl_2$ eutectic salt. Ceram. Int. **42**, 7852–7856 (2016)

20. J. Liu, Y. Wang, X. Yu, J. Li, Enhanced photoluminescence properties of $Zn_2SiO_4$:$Mn^{2+}$ co-activated with $Y^{3+}$/$Li^{+}$ under VUV excitation. J. Luminescence. **130**, 2171 (2010)
21. R.G. Singh, F. Singh, R.M. Mehra, D. Kanjilal, V. Agarwal, Synthesis of nanocrystalline α-$Zn_2SiO_4$ at ZnO—porous silicon interface: Phase transition study. Solid State Commun. **151**, 701–703 (2011)
22. A. Patra, G.A. Baker, S.N. Baker, Effects of dopant concentration and annealing temperature on the phosphorescence from $Zn_2SiO_4$:$Mn^{2+}$ nanocrystals. J. Luminescence. **111**, 105–111 (2005)
23. K. Omri, L. El, Mir, Effect of manganese concentration on photoluminescence properties of $Zn_2SiO_4$:Mn nanophosphor material. Superlattices Microstruct. **70**, 24–32 (2014)
24. C.M. Lin, Y.Z. Tsai, J.S. Chen, The microstructure and cathodoluminescence characteristics of sputtered $Zn_2SiO_4$:Ti phosphor thin films. Thin Solid Films. **515**, 7994–7999 (2007)
25. D.M. de Leeuw, G.W. Hooft, Method for the analysis of saturation effects of cathodoluminescence in phosphors; applied to $Zn_2SiO_4$:Mn and $Y_3Al_5O_{12}$:Tb. J. Luminescence. **28**, 275–300 (1983)
26. H. Li, G. Liu, J. Wang, X. Dong, W. Yu, $Eu^{3+}$/$Tb^{3+}$ doped cubic BaGdF5 multifunctional nanophosphors: Multicolor tunable luminescence, energy transfer and magnetic properties. J. Luminescence. **186**, 6–15 (2017)